Automated Segmentation and Classification of Multispectral Magnetic Resonance Images of Brain Using Artificial Neural Networks

Wilburn E. Reddick,* *Member, IEEE*, John O. Glass, *Student Member, IEEE*, Edwin N. Cook, T. David Elkin, and Russell J. Deaton, *Member, IEEE*

***Abstract*—We present a fully automated process for segmentation and classification of multispectral magnetic resonance (MR) images. This hybrid neural network method uses a Kohonen self-organizing neural network for segmentation and a multilayer backpropagation neural network for classification. To separate different tissue types, this process uses the standard T1-, T2-, and PD-weighted MR images acquired in clinical examinations. Volumetric measurements of brain structures, relative to intracranial volume, were calculated for an index transverse section in 14 normal subjects (median age 25 years; seven male, seven female). This index slice was at the level of the basal ganglia, included both genu and splenium of the corpus callosum, and generally, showed the putamen and lateral ventricle. An intraclass correlation of this automated segmentation and classification of tissues with the accepted standard of radiologist identification for the index slice in the 14 volunteers demonstrated coefficients (r_i) of 0.91, 0.95, and 0.98 for white matter, gray matter, and ventricular cerebrospinal fluid (CSF), respectively. An analysis of variance for estimates of brain parenchyma volumes in five volunteers imaged five times each demonstrated high intrasubject reproducibility with a significance of at least $p < 0.05$ for white matter, gray matter, and white/gray partial volumes. The population variation, across 14 volunteers, demonstrated little deviation from the averages for gray and white matter, while partial volume classes exhibited a slightly higher degree of variability. This fully automated technique produces reliable and reproducible MR image segmentation and classification while eliminating intra- and interobserver variability.**

***Index Terms*—Image processing, image segmentation and classification, MRI, neural networks.**

Manuscript received October 11, 1996; revised August 29, 1997. This work was supported in part by the National Cancer Institute under Cancer Center Support (CORE) Grant P30CA21765 and by the American Lebanese Syrian Associated Charities (ALSAC). The Associate Editor responsible for coordinating the review of this paper and recommending its publication was M. W. Vannier. *Asterisk indicates corresponding author.*

*W. E. Reddick is with the Department of Diagnostic Imaging, St. Jude Children's Research Hospital, 332 N. Lauderdale, Memphis, TN 38105 USA (e-mail: gene.reddick@stjude.org). He is also with the Departments of Electrical Engineering and Biomedical Engineering, University of Memphis, Memphis, TN 38152 USA.

J. O. Glass is with the Departments of Diagnostic Imaging, St. Jude Children's Research Hospital, Memphis, TN 38105 USA.

E. N. Cook is with the Department of Radiology, University of Tennessee School of Medicine, Memphis, TN 38152 USA.

T. D. Elkin is with the Department of Behavioral Medicine, St. Jude Children's Research Hospital, Memphis, TN 38105 USA. He is also with the Department of Psychology, University of Memphis, Memphis, TN 38152 USA.

R. J. Deaton is with the Department of Electrical Engineering, University of Memphis, Memphis, TN 38152 USA.

Publisher Item Identifier S 0278-0062(97)09342-7.

I. Introduction

SEGMENTATION and classification of brain parenchyma is a promising method for addressing a wide range of clinical problems, such as longitudinal assessments of therapy response, long-term sequelae of treatment, and improved detection of subtle brain pathology [1]–[6]. A fully automated method gains in both reliability and clinical acceptance, by the elimination of both intra- and inter-observer variability. Two of the earliest reports of magnetic resonance (MR) image segmentation used multispectral images to accentuate the differences in physical characteristics of the anatomical tissues [7], [8]. Recent developments in magnetic resonance imaging (MRI) system design have resulted in significant advances in the quality, stability, and speed of imaging procedures. Segmentation of MR images has become an increasingly vital area of research, resulting in numerous publications in the last three years.

A computer-vision paradigm submits the input image to a series of processes: preprocessing, feature extraction, segmentation, and classification. Preprocessing improves the quality of the input images by accurate registration [9], correction of field inhomogeneities [10], [11], and noise filtering [12]–[15]. Image segmentation refers to the decomposition of an image into regions, while classification is the step that labels each of these regions by tissue type. This association is most commonly performed by the operator or interpreted by the physician. A comprehensive review of MRI segmentation methods [16] and the theoretical basis of these methods [17] have recently been presented. Feature extraction is a common approach for multispectral MRI segmentation and can be either supervised or unsupervised. Supervised methods require operator input for segmentation [18]–[24], while unsupervised methods are automatic [25]–[29]. Operator intervention may be necessary to complete the process, but the result should be operator independent.

Neural networks, with both supervised [30] and unsupervised [31]–[34] learning methods, have been used to segment MR images. Neural networks have demonstrated superior performance over classical maximum likelihood methods when small training sets are used. The major advantage of neural network methods over classical statistical pattern recognition methods is the relative insensitivity to selection of the training sets afforded by generalization [30]. A semiautomatic tech-

nique, developed by Raff *et al.*, used a perceptron neural network to segment gray and white matter based on proton-density weighted images. This method demonstrated accuracy to within 7% for individual slices compared to segmentation by a trained neuroradiologist [32]. However, reliable and reproducible quantitation can be achieved only through fully automated techniques. Unsupervised segmentation methods, such as the Hopfield neural network, are fast to converge and have shown promising results compared to hard and fuzzy c-means methods [31], [34]. Generalization of learning vector quantization (LVQ) was explicitly designed as a clustering algorithm for segmentation that updates all nodes for a given input vector [33]. This modified algorithm was based on Kohnonen's initial study with LVQ and self-organizing maps (SOM). The generalized LVQ method was relatively invariant to number of iterations, learning coefficients, and initialization. All of these methods have concentrated on the segmentation task and have not addressed the classification issue. However, there have been two reports of combining an unsupervised fuzzy c-means clustering segmentation algorithm with an expert system to perform the classification task [25], [26].

We have developed a fully automated, novel MR image segmentation and classification technique based entirely on artificial neural networks. This technique uses T1-weighted (T1), T2-weighted (T2), and proton density-weighted (PD) MR images as inputs. An unsupervised artificial neural network, the Kohonen self-organizing map [35], [36], segments the MR images into regions of similar image characteristics. Haring *et al.* have shown that the Kohonen SOM is capable of segmenting MR images using a multiscale approach with a single T1 image [37]. We have expanded this work by incorporating a multispectral approach. This process exploits the signal intensity variations radiologists use to identify tissue types. A second, multilayer backpropagation neural network then classifies the tissue types of each segmented region. We assess the reproducibility of the technique for segmenting and classifying brain images obtained from multiple examinations of a single volunteer and from a group of 14 volunteers. This technique provides reliable and reproducible MR image segmentation and classification, which eliminates intra- and inter-operator variability.

II. Methods

A. Volunteers

Fourteen normal healthy volunteers (seven female, seven male; aged 20–32 years [median: 25 years]) were recruited from a population of hospital personnel for this study. All volunteers underwent imaging protocols approved by the hospital's Institutional Review Board after informed consent was obtained.

B. MR Imaging

All MR imaging of subjects was performed on 1.5-T SP63 Magnetom (Siemens Medical Systems, Iselin, NJ) whole body imagers using the standard circular polarized volume head coil. A localizer sequence was used to determine subject position in the coil for subsequent imaging. All images were acquired as transverse 5-mm-thick slices with a 1-mm-gap between slices, and were interleaved to avoid crosstalk between slice excitations. T1-weighted images were acquired using a gradient-echo FLASH-2D imaging sequence (TR/TE = 266/6 ms, 90° flip angle, 192 phase encodes, three acquisitions). T2-weighted and PD-weighted images were acquired simultaneously using a dual spin-echo sequence (TR/TE1/TE2 = 3500/19/93 ms, two echoes, 192 phase encodes, one acquisition). We chose these two sequences because they are routinely obtained as part of clinical imaging for patients with brain tumors. Standard positioning beams on the magnet and head immobilization devices built into the head coil by the manufacturer were sufficient to ensure adequate head positioning and immobilization in these studies.

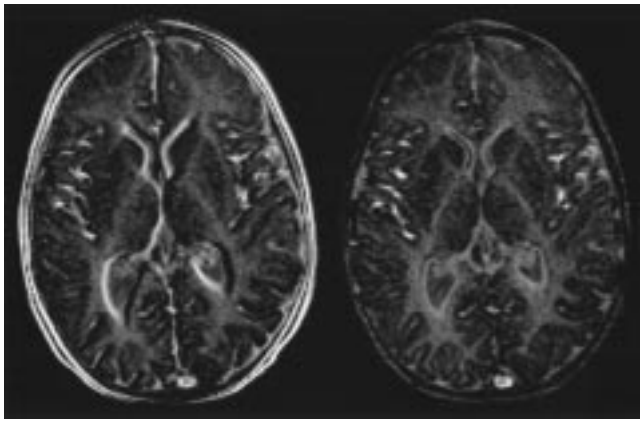

Fig. 1. The difference image, shown on left, demonstrates a misaligned T1 and T2/PD imaging set caused by patient movement during the examination. The difference image after registration is shown on right.

Registration of the two imaging sequences used to acquire the segmentation data (T1 and T2/PD) was checked for every examination and corrected when necessary. Registration (2D) was accomplished with a landmark matching method using internal anatomical landmarks identified by a trained expert. The registration method, based on the Procrustes algorithm, finds the least-squared solution by minimizing the distance among all paired points [38]. As a demonstration of the technique, a difference image for a misaligned patient examination is shown in Fig. 1 along with the difference image after realignment.

The complete imaging set was reviewed to select the image which best exhibited the anatomical structures of interest. A single transverse section at the level of the basal ganglia, including both genu and splenium of the corpus callosum, and generally, showing the putamen and the lateral ventricle was selected as the index slice for this investigation. This representative index slice was chosen to sample cortical gray matter, white matter, central gray matter structures, and ventricular cerebrospinal fluid (CSF). The thickness of the imaging slices does not allow for reliable visualization of fine structures such as the intervening white matter tract between the putamen and globus pallidus. Segmentation of such fine structures would be improved with optimized image acquisition.

The image set submitted to the segmentation procedure consisted of the index slice plus the adjacent superior and

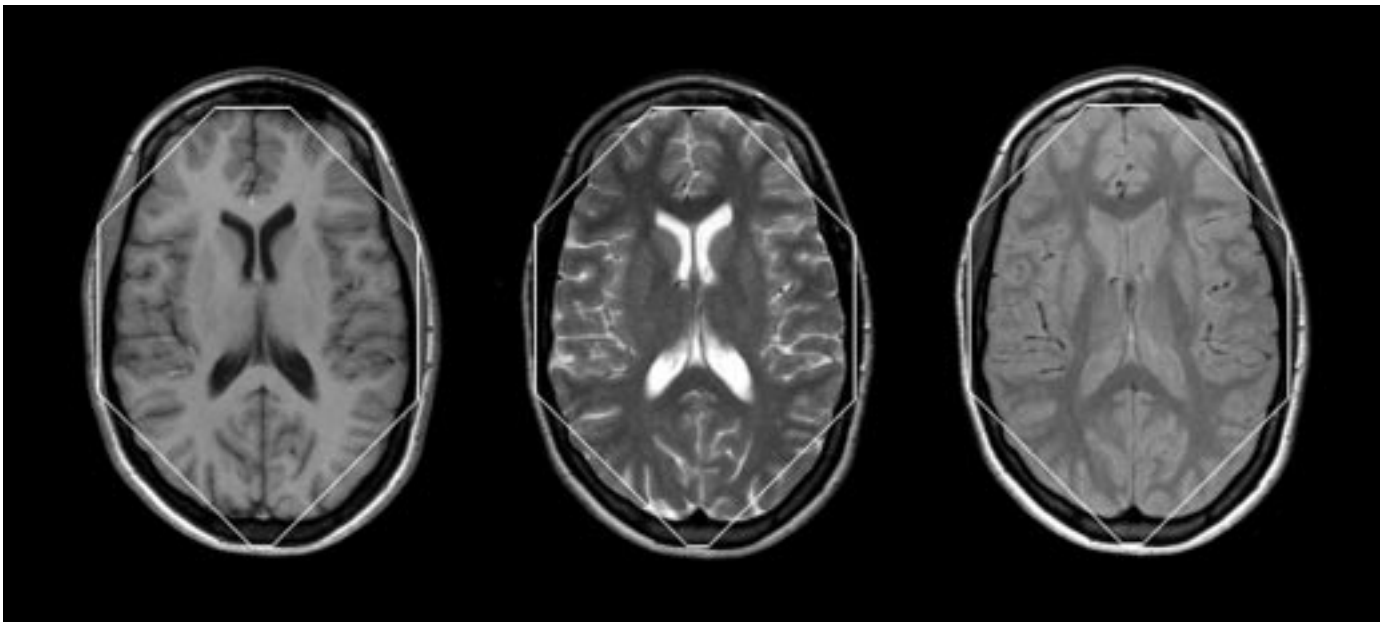

Fig. 2. Input images to unsupervised segmentation neural network. The images shown, at level of index slice, are T1-weighted (left), T2-weighted (center), and PD-weighted (right) for a typical volunteer. Only the image data within the automatically defined octagonal region of interest was used to train the segmentation network.

inferior sections. Each of these images was preprocessed with a custom algorithm to remove much of the extrameningeal tissue and background from further analysis. This step consisted of an initial threshholding of the T1 image at an empirically determined level to eliminate almost all of the background pixels in the image. A line scan histogram was then determined for horizontal, vertical, positive, and negative diagonal directions. To eliminate extrameningeal tissues, an acceptance criteria was set at 50% of the histogram maximum. This produced two cutoffs, one on each side of the histogram. The T1 image was chosen for this procedure because of the greater contrast between the high signal from subcutaneous fat and the corresponding low signal from the skull. Excluding all pixels beyond the two line scan histogram cutoffs for each of the four directions yielded an automatically-selected octagonal region of interest which was predominantly brain parenchyma with very little extrameningeal tissue. The region of interest determined for the T1 image was applied to the T2 and PD images at the same slice position, as shown in Fig. 2 for all three input images. This technique effectively eliminated excessive background signals and, therefore, reduced the execution time of the overall segmentation and classification process.

C. SOM Segmentation Design

Our segmentation method utilized a Kohonen self-organizing map [35], [36], shown in Fig. 3. In the SOM, a competitive learning algorithm adjusts vectors of weights, $\boldsymbol{w_i} = \{w_i, 1, w_i, 2, \cdots, w_i, j\}$, which are associated with each unit or neuron, to form a representation of a space of N input vectors, $\mathbf{input_k} = \{\mathrm{input}_1, \cdots, \mathrm{input}_j\}$, where $k = 1, \cdots N$. Through a neighborhood function, the topology of the input space is preserved in the SOM representation. In other words, similar inputs are represented by neurons that are close in the SOM. A typical measure of distance is the Euclidean metric.

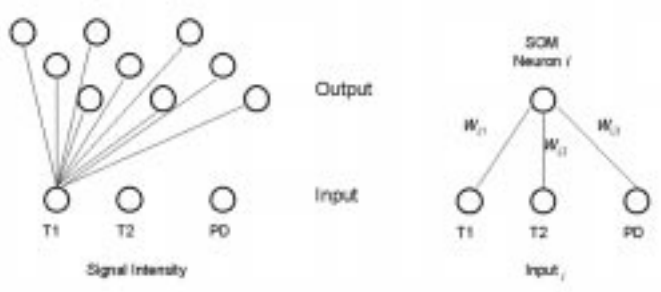

Fig. 3. An example of the SOM used in this study, with three input and nine fully connected output neurons is shown on the left. The three inputs correspond to the signal intensities from a single pixel in a T1-weighted, T2-weighted and PD magnetic resonance images. A more detailed view of the weight vector associated with SOM neuron i is shown on the right for an input vector j.

For this application, a three unit input vector, $\mathbf{input_k}$, is composed of the nonnormalized T1, T2, and PD signal intensities for a single pixel in the MR image. The input vectors were initialized with a standard set of average signal intensities (T1, T2, and PD) for white matter, gray matter, and CSF. This standard initialization set of average values was previously determined for five randomly selected examinations not used in this investigation. The SOM configuration was a single layer of nine neurons arranged in a three by three topology. Nine neurons allow sufficient capacity for multiple classes of tissue to be defined before collapsing to the final seven segmented tissue and background regions expected in normal brain parenchyma. In order to reduce running time while providing an ample number of meaningful tissue classifications, the SOM geometry was selected in preference to a multilayered geometry.

All pixels within the region of interest for the index slice and the adjacent superior and inferior sections were mapped from

the input space of the combined multispectral pixel intensities to an output space. This output space was identified by the designation, i, of the output neuron whose connection weights ($\boldsymbol{w_i}$) most closely matched the given input vector ($\mathbf{input_k}$), as measured in a Euclidean metric. The winning neuron's weights were changed by

$$\Delta \text{ weight}_{i,j} = \text{neigh(iter)}[\text{input}_j - \text{weight}_{i,j}] \quad (1)$$

while the weights of all other neurons were changed by the quantity

$$\Delta \text{ weight}_{i,j} = (\text{neigh(iter)})^2[\text{input}_j - \text{weight}_{i,j}] \quad (2)$$

where input_j is the input corresponding to the three types of pixel intensities, $w_{i,j}$ is the weight (see Fig. 3), j is an index for each of the three elements of the input vector, and i is the index for the nine neurons.

The neighborhood function used in this experiment was a Gaussian of the form

$$\text{neigh(iter)} = \eta * \exp\left[\frac{-(x^2+y^2)}{2*\sigma^2}\right] \quad (3)$$

where

$$\eta = 0.005^{\text{iter}/\text{iter}_{\max}} \quad (4)$$

and

$$\sigma = 3(0.4^{\text{iter}/\text{iter}_{\max}}) \quad (5)$$

which was chosen to ensure the convergence of the weight vectors to meaningful outputs. The distance between the winning neuron and the updated neuron is represented as $(x^2 + y^2)$, where x and y are the coordinate differences in the two dimensions of the output plane. The variable iter represents the iteration that the algorithm is currently executing while $\text{iter}_{\max}$ is a user defined ending criteria. The monotonically decreasing form of the neighborhood function ensures that the SOM procedure will converge to a final set of prototypical vectors. However, the utility of these vectors is not guaranteed. For instance, if the neighborhood function is decreased too rapidly, the weight vectors may only segment brain and CSF rather than differentiate gray and white matter. Five-hundred iterations were determined empirically to be sufficient to ensure reliable convergence of the weight vectors to meaningful outputs for the data collected in this study. Once the SOM process was trained on the input vectors within the region of interest, all input vectors from the entire three sections were then presented to the trained SOM for a final pass. In this last step in the segmentation process, all input vectors were assigned to one of the nine SOM neurons. The SOM process executes in approximately 16 min on an SGI Indy R5000 (Silicon Graphics Incorporated, Mountain View, CA) Unix workstation.

D. Classification Design

After segmentation was completed, each of the nine levels in the segmented images were classified according to tissue type using an Apple Macintosh IIvx computer running Adobe Photoshop version 2.5.1. Seven of the labeled studies were then used to train, and the remaining seven were used to test a second artificial neural network for automated classification.

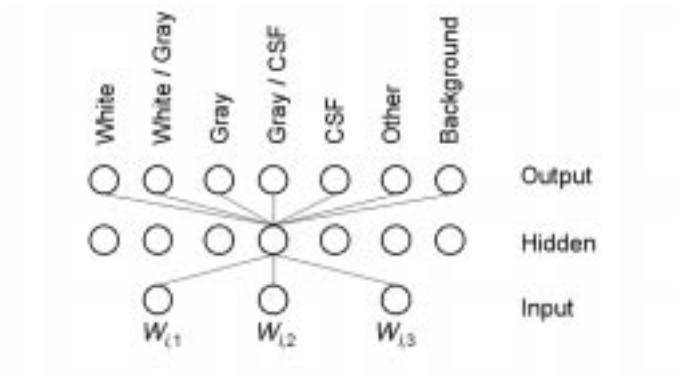

Fig. 4. The fully connected multilayer backpropagation neural network used in this study is illustrated with three input, seven hidden and seven output neurons. The three inputs correspond to the components of the weight vector associated with a single SOM neuron representing the segmented region to be classified. The seven output neurons correspond to brain parenchyma tissue types or partial volumes of tissue types.

In the second artificial neural network, a three-layer feed-forward network (shown in Fig. 4) was trained with error backpropagation utilizing the generalized delta rule for learning. The input layer included three neurons with a linear transfer function, while both the hidden layer and the output layer had seven neurons with sigmoid transfer functions. All neurons were fully connected between layers, and the initial connection vectors were randomized between one and negative one. The learning rate for the network was set to a value of 0.1, and the momentum factor was set to 0.5. The network was trained with the inputs being presented randomly each cycle.

The three input neurons of the classification network corresponded to the three components of the weight vector associated with each neuron of the SOM network. The 14 volunteer data sets were randomly divided into two groups of seven sets, a training and a testing set. The weight vectors from the segmentation procedure were normalized by a constant scale factor of 600 such that maximum values were approximately one before being submitted to the classification network. Each input vector into the classification network had an associated manual classification, which corresponded to one of the seven labels for intracranial tissue or background.

The seven classification labels were mapped to a color scheme, similar to that previously used for positron emission tomography (PET) to display the images in a color format. Fig. 5 shows a color-coded image segmentation of the input images shown in Fig. 2. Gray matter tissues were colored yellow to emphasize their relatively high metabolic activity compared to the less active white matter tissues, which were colored green. Partial volumes of gray and white matter were colored a yellow-green to emphasize their dual components. Partial volumes of CSF and gray matter were colored medium blue, while CSF was colored a light blue. Blood vessels and membranes were colored a dark violet.

E. Validation Techniques

1) Classification: Examinations of 57 patients with no neurological abnormalities in the index slice were used to test

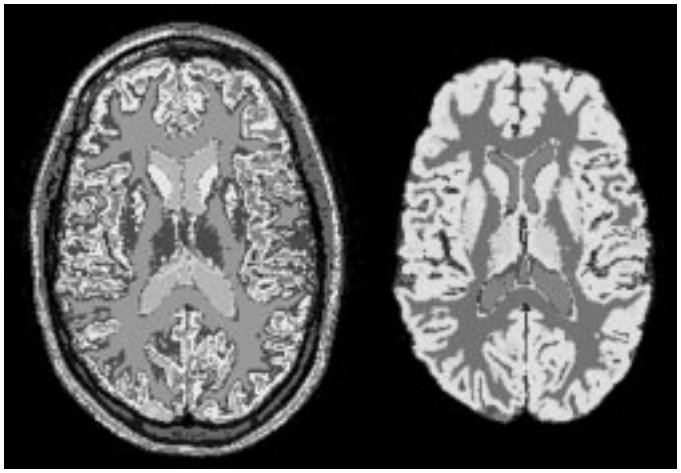

Fig. 5. The nine-level gray scale image, shown on left, represents segmentation of input images shown in Fig. 2. A pseudocolor display of classification results is shown on right. While only the image data within the octagonal region of interest was used to train the segmentation network, the entire image was submitted for complete segmentation and classification. The extrameningeal tissues (including scalp, subcutaneous fat, muscle, and calvarium) in the color-coded results were manually removed for presentation.

the generalization of the classification algorithm on data not used in training. The testing set contained 513 vectors corresponding to the weight vectors associated with each neuron of the SOM for all 57 examinations. The segmented index image for each of the 57 patients had nine segmented regions corresponding to the nine prototypical weight vectors. These images (Fig. 5, left) were displayed and each segmented region manually labeled by the radiologist by tissue type. This manual classification of the regions and their corresponding prototypical vectors was considered ground truth for testing the classification network.

2) Segmentation: The judgments of a radiologist (E. N. Cook) were used to determine the accuracy of the segmentation technique, as this is the most acceptable criterion for *in vivo* evaluation of the tissue type of brain parenchyma [16]. Operator variability in selection of brain volumes have been previously reported by several investigators as 1–4% for intraobserver and 1–21% for interobserver [19], [39]–[41]. The validation studies in this investigation were performed only once by a single radiologist and, therefore, were not evaluable for observer variability. The radiologist manually selected the regions corresponding to gray matter, white matter, and ventricular CSF for the slice of interest in each of the 14 studies, using a graphical interface on a Silicon Graphics Indy workstation. For this study, the volumes identified as partial white and gray matter were combined with the gray matter volumes. This collapsing of the segmented regions was necessary for the validation study because many of the deep gray structures were classified by the neural network as partial volumes of white and gray matter. This discrepancy is attributed to the T1 relaxation rate of putamen (853 ms) and thalamus (775 ms) occurring between the T1 rates of white matter (571–590 ms) and gray matter (1026 ms). Volumes identified by the neural network as partial gray matter and CSF were considered neither gray matter nor ventricular CSF. Table I clarifies the comparison of automatically segmented regions with radiologist's selected regions. These selected regions were compared to the color scheme output of the segmentation algorithm for a pixel by pixel evaluation, allowing for a comparison of pixel number as well as placement for the various tissue types. An intraclass correlation analysis was performed to compare the two techniques.

TABLE I
MAPPING OF AUTOMATICALLY SEGMENTED REGIONS FROM HYBRID NEURAL NETWORK (6) TO MANUALLY SEGMENTED REGIONS BY RADIOLOGIST (3) FOR VALIDATION STUDY

Radiologist	Hybrid Neural Network
White Matter	White Matter
Gray Matter	Gray Matter + White / Gray
CSF	CSF
Incorrect	Gray / CSF + Other

III. RESULTS AND DISCUSSIONS

A. Classification Validation

The testing procedure of the classification network was the process through which each segmented region was classified by tissue type. The amount of error was determined by the number of misclassifications, compared to manual classifications, in the testing procedure for each set of inputs. A misclassification occurs when the neural network classification of a segmented region disagrees with manual identification of the region. Testing of the classification network with 57 patient examinations demonstrated an overall misclassification of only 11.3% (58/513) when validated against manual classification. This error indicates that only 58 of the 513 segmented regions were incorrectly labeled by the classification network. The backpropagation neural network was both an accurate (88.7%) and reproducible method for classifying segmented tissue types using the weight vectors associated with each SOM neuron. However, the existence of any error emphasizes the continued need for human supervision and verification of results, even for fully automated procedures. Within the confidence limits shown, the classification neural network reduces the amount of user bias in subsequent examinations. All classifications used in the segmentation validation and analysis of variance were manually verified by an expert.

B. Hybrid Neural Network Validation

There are several methods available to validate the performance of segmentation techniques used to analyze medical images of brain parenchyma [16]. The best *in vivo* assessment of brain parenchyma remains the manual selection by a radiologist trained in neurological MRI. The radiologist (E. N. Cook) selected regions of white matter, gray matter, and ventricular CSF from T1, T2, and proton density images of the index slice in each of the 14 volunteers. These classifications were then compared to the maps created by the automated neural network segmentation and classification using an intraclass correlation analysis. An intraclass correlation is a measure of correlation between raters and provides an indication of the reliability of

ratings (segmentation and classification) [42]. For this analysis, the radiologist was the first rater and the hybrid neural network the second. The analysis was performed using 14 comparison sets composed of the index images from the 14 volunteers and yields a single intraclass correlation coefficient for each tissue type.

The intraclass correlation coefficients (r_i) were 0.91, 0.95, and 0.98 for white matter, gray matter, and ventricular CSF, respectively. All intraclass correlations were statistically significant with $p < 0.001$. The coefficient for white matter was lower than gray matter although the shape and distribution of gray matter is more complex. This lower coefficient may be due to the combination of the partial gray/white with the gray matter classification. The highest correlation coefficient was expressed by ventricular CSF whose simple shape and distribution in the index slice was easily identified by the radiologist on T2-weighted images.

The validation studies were performed only once by a single radiologist and, therefore, were not evaluable for observer variability. Previous investigators have reported intraobserver variations ranging from 1–4%. This source of error was not evaluated but would cause some small variation in the reported correlations. However, since the correlation coefficients were highly significant for all three tissues, this variance is unlikely to diminish the impact of the study.

All images used in this study were 5-mm thick. These relatively thick slices accounted for partial volume effects seen in both the thickness of the gray/white matter interface and in the existence of the partial gray/CSF region. While the boundary between gray and white matter was a graded interface with a thin translational region between the tissue types, the gray matter and CSF boundary was a discrete interface between tissue and fluid. The existence of the partial gray/CSF region exemplified the difficulty in segmenting curved boundaries with thick slices. This hybrid neural network method for automated segmentation and classification was developed with a pilot study of imaging examinations which were in standard clinical use at our institution and were not optimized for volumetric measurements. We are currently developing an optimized imaging procedure, which will acquire field corrected 1 mm thick contiguous slices of the whole brain. However, the studies presented demonstrate the accuracy of the neural network technique and emphasize the feasibility of the technique on actual MR examinations performed on a clinical imager.

C. Analysis of Variance

To investigate the reproducibility of our method, five subjects were imaged five times each. In order to investigate intrasubject reliability we used an analysis of variance. The intrasubject variation by tissue type for the five studies showed little variation, as demonstrated in Table II.

White matter, white/gray matter, and CSF were all highly reproducible measures in these five subjects. Gray matter was less reproducible but still significant with $p < 0.05$. The cortical gray matter exhibits both complex shape and distribution. In addition, segmentation of the gray matter would be most susceptible to the coil sensitivity profile. Reproducibility measures of CSF/gray matter partial volumes approached statistical significance. The lower reproducibility can be accounted for by the influence of thick imaging slices. Slight variations in patient positioning would cause variations in the degree of partial voluming, especially around the sulci where CSF/gray matter contamination occurs.

TABLE II
ANALYSIS OF VARIANCE FOR INTRASUBJECT REPRODUCIBILITY STUDY OF FIVE VOLUNTEERS IMAGED FIVE TIMES EACH. THE UNIVARIATE F-TESTS WITH (4,20) DEGREES OF FREEDOM ARE SHOWN WITH THE MEASURE OF SIGNIFICANCE FOR F

	F(4,20)	p
White Matter	24.32	<0.001
White / Gray	9.69	<0.001
Gray Matter	3.68	0.021
Gray / CSF	2.33	0.091
CSF	57.65	<0.001

TABLE III
ANALYSIS OF INTERSUBJECT VARIATION BY TISSUE TYPE. ALL VOLUMES ARE FROM THE INDEX SLICE AND HAVE BEEN NORMALIZED TO INTRACRANIAL VOLUME IN THE INDEX SLICE. THE MEAN AND STANDARD DEVIATION OF TISSUE VOLUMES ARE REPORTED $(N = 14)$

White Matter	0.285 ± 0.031
White / Gray	0.183 ± 0.063
Gray Matter	0.376 ± 0.069
Gray / CSF	0.082 ± 0.026
CSF	0.044 ± 0.017
Other	0.031 ± 0.015

The small variations seen in this reproducibility study represent the true amount of error involved with the segmentation process, including errors in patient repositioning and finite slice thickness. The hybrid neural network appears to be reliable across most tissue types. With this level of intrasubject variance, segmentation and classification of serial examinations on patients would be feasible. Such automated segmentation analysis of serial examinations on patients may yield important new measures of subtle disease effects or response to treatment.

An investigation of the 14 volunteers was conducted to demonstrate the range of variations in segmented brain parenchyma volumes that could be expected between subjects for the index slice. The volume for each tissue was normalized to intracranial volume in the index slice. This normalization removes the variance due to differences in head size across the population. The average and standard deviation for each tissue volume were shown in Table III. Pure tissue volumes such as white and gray matter demonstrated little deviation from the average for the population sampled. The CSF volumes, however, exhibited a high degree of variability. True variation in ventricular size accounts for most of this variation, because CSF volumes were shown highly reproducible in the same patient. Another possible factor was head positioning. Ventricular volumes in a single slice can vary largely with the orientation of the imaging plane. Relatively large variations were observed for both CSF/gray and gray/white matter partial volume classes. These results display the sensitivity

of the segmentation and classification algorithms in detecting abnormal variations in a heterogeneous population. The distributions of the various brain tissue volumes for the volunteers emphasize the possible clinical application of this technique for examining relative volumes in patients.

IV. Summary and Conclusions

This paper presents a hybrid Kohonen self-organizing map/multilayer backpropagation neural network technique for unsupervised segmentation and classification of MR brain images. The only preprocessing performed was the automated removal of extrameningeal tissues. Inclusion of additional preprocessing procedures, such as correction of RF field inhomogeneities, could potentially improve the performance of this technique.

Several unsupervised neural network and statistical techniques have been reported for segmentation of MR images, but many of these rely on assumed distribution functions [28], [29], [31], [32] and do not address classification of the segmented regions. Expert systems for automated classification of segmented regions have been combined with fuzzy c-means segmentation, which is an unsupervised technique [25], [26]. This classification technique used anatomical templates and *a priori* knowledge of boundaries and tissue signatures to classify the segmented regions. Likewise, the hybrid neural network technique relies on the tissue signatures used to train the backpropagation network. However, no spatial constraints were imposed on the neural network classification. More than one segmented region could be classified as the same tissue type, such as two regions of white matter, without requiring conditional processing for this special case.

The hybrid neural network technique includes identification of regions of partial volume contamination and exhibits a high degree of accuracy with radiologist selected regions. An intraclass correlation of this automated segmentation and classification of tissues with the accepted standard of radiologist identification demonstrated coefficients (r_i) of 0.91, 0.95, and 0.98 for white matter, gray matter, and ventricular CSF, respectively. The robustness and reproducibility of the hybrid technique was demonstrated for a single index image in volunteer studies. An analysis of variance for estimates of brain parenchyma volumes in five volunteers imaged five times each demonstrated excellent intrasubject reproducibility with a significance of at least $p < 0.05$ for white matter, gray matter, and white/gray partial volumes. The population variation, across 14 volunteers, demonstrated little deviation from the averages for gray and white matter, while partial volume classes exhibited a slightly higher degree of variability.

At our institution, this technique is being used in a pilot study of medulloblastoma patients receiving cranial irradiation to quantitatively assess white matter loss. Children surviving medulloblastoma have learning and memory deficits that are particularly problematic. It is hypothesized that these deficits are secondary to radiation-induced loss of either normal white or gray matter. This hybrid neural network technique is a promising tool for addressing a wide range of clinical problems, such as long-term sequelae of treatment.

Acknowledgment

The authors would like to thank neuroradiologist J. W. Langston, MD, for advice in the development of the validation procedures and color scheme for presentation of segmentation and classification results. They would also like to thank J. S. Taylor, Ph.D., for advice and encouragement throughout this process.

References

[1] R. L. Galloway, Jr., R. J. Maciunas, and A. L. Failinger, "Factors affecting perceived tumor volumes in magnetic resonance imaging," *Ann. Biomed. Eng.*, vol. 21, pp. 367–375, 1993.

[2] P. A. Narayana, E. F. Jackson, and J. S. Wolinsky, "Inter- and intraoperator variability in the quantitative volumetric measurements of multiple sclerosis lesions," *J. Magn. Reson. Imag.*, (Supp.), vol. 3, pp. 111–112, 1993. (Abstract)

[3] T. Taxt, A. Lundervold, B. Fuglaas, H. Lien, and V. Abeler, "Multispectral analysis of uterine corpus tumors in magnetic resonance imaging," *Magn. Reson. in Med.*, vol. 23, pp. 55–76, 1992.

[4] R. P. Velthuizen, L. P. Clarke, S. Phuphanich, L. O. Hall, A. M. Bensaid, J. A. Arrington, H. Greenberg, and M. L. Silbiger, "Unsupervised measurement of brain tumor volume on MR images," *J. Magn. Reson. Imag.*, vol. 5, pp. 594–605, 1995.

[5] S. C. Carpentieri, R. K. Mulhern, S. Douglas, S. Hanna, and D. L. Fairclough, "Behavioral resiliency among children surviving brain tumors: A longitudinal study," *J. Clin. Child Psychol.*, vol. 22, pp. 236–246, 1993.

[6] E. H. Aylward, P. D. Brettschneider, J. C. McArthur, G. J. Harris, T. E. Schlaepfer, J. D. Henderer, P. E. Barta, A. Y. Tien, and G. D. Pearlson, "Magnetic resonance imaging measurements of gray matter volume reductions in HIV dementia," *Amer. J. Psych.*, vol. 152, pp. 987–994, 1995.

[7] M. W. Vannier, R. L. Butterfield, D. Jordan, W. A. Murphy, R. G. Levitt, and M. Gado, "Multispectral analysis of magnetic resonance images," *Radiol.*, vol. 154, pp. 221–224, 1985.

[8] R. Bachus, H. Konig, G. Lenz, M. Deimling, and E. R. Reinhardt, "Tissue differentiation in MRI by means of pattern recognition," *Comput. Assist. Radiol.*, vol. pp. 496–501, 1985.

[9] C. R. Meyer, G. S. Leichtman, J. A. Brunberg, R. L. Wahl, and L. E. Quint, "Simultaneous usage of homologous points, lines, and planes for optimal, 3-D, linear registration of multimodality imaging data," *IEEE Trans. Med. Imag.*, vol. 14, pp. 1–11, 1995.

[10] C. R. Meyer, P. H. Bland, and J. Pipe, "Retrospective correction of intensity inhomogeneities in MRI," *IEEE Trans. Med. Imag.*, vol. 14, pp. 36–41, 1995.

[11] B. M. Dawant, A. P. Zijdenbos, and R. A. Margolin, "Correction of intensity variations in MR images for computer-aided tissue classification," *IEEE Trans. Med. Imag.*, vol. 12, pp. 770–781, 1993.

[12] K. Ying, B. Clymer, and P. Schmalbrock, "Adaptive filtering processing for magnetic resonance images," in *Proc. Soc. Magnetic Resonance*, 2nd Meeting, pp. 803, 1994. (Abstract)

[13] G. Gerig, O. Kubler, R. Kikinis, and F. A. Jolesz, "Nonlinear anisotropic filtering of MRI data," *IEEE Trans. Med. Imag.*, vol. 11, pp. 221–232, 1992.

[14] M. Tincher, C. R. Meyer, R. Gupta, and D. M. Williams, "Polynomial modeling and reduction of RF body coil spatial inhomogeneity in MRI," *IEEE Trans. Med. Imag.*, vol. 12, pp. 361–365, 1993.

[15] A. Simmons, S. R. Arridge, G. J. Barker, A. J. Cluckie, and P. S. Tofts, "Improvements to the quality of MRI cluster analysis," *Magn. Reson. Imag.*, vol. 12, pp. 1191–1204, 1994.

[16] L. P. Clarke, R. P. Velthuizen, M. A. Camacho, J. J. Heine, M. Vaidyanathan, L. O. Hall, R. W. Thatcher, and M. L. Silbiger, "MRI segmentation: Methods and applications," *Magn. Reson. Imag.*, vol. 13, pp. 343–368, 1995.

[17] J. C. Bezdek, L. O. Hall, and L. P. Clarke, "Review of MR image segmentation techniques using pattern recognition," *Med. Phys.*, vol. 20, pp. 1033–1048, 1993.

[18] H. E. Cline, W. E. Lorensen, S. P. Souza, F. A. Jolesz, R. Kikinis, G. Gerig, and T. E. Kennedy, "3-D surface rendered MR images of the brain and its vasculature," *J. Comput. Assist. Tomogr.*, vol. 15, pp. 344–351, 1991.

[19] M. I. Kohn, N. K. Tanna, G. T. Herman, S. M. Resnick, P. D. Mozley, R. E. Gur, A. Alavi, R. A. Zimmerman, and R. C. Gur, "Analysis of

brain cerebrospinal fluid volumes with MR imaging," *Radiol.*, vol. 178, pp. 115–122, 1991.
[20] K. J. McClain, Y. Zhu, and J. D. Hazle, "Selection of MR images for automated segmentation," *J. Magn. Reson. Imag.*, vol. 5, pp. 485–492, 1995.
[21] D. D. Blatter, E. D. Bigler, S. D. Gale, S. C. Johnson, C. V. Anderson, B. M. Burnett, N. Parker, S. Kurth, and S. D. Horn, "Quantitative volumetric analysis of brain MR: normative database spanning five decades of life," *Amer. J. Neuroradiol.*, vol. 16, pp. 241–251, 1995.
[22] L. M. Fletcher, J. B. Barsotti, and J. P. Hornak, "A multispectral analysis of brain tissues," *Magn. Reson. in Med.*, vol. 29, pp. 623–630, 1993.
[23] M. Kamber, R. Shinghal, D. L. Collins, G. S. Francis, and A. C. Evans, "Model-based 3-D segmentation of multiple sclerosis lesions in magnetic resonance brain images," *IEEE Trans. Med. Imag.*, vol. 14, pp. 442–453, 1995.
[24] T. Taxt and A. Lundervold, "Multispectral analysis of the brain using magnetic resonance imaging," *IEEE Trans. Med. Imag.*, vol. 13, pp. 470–481, 1994.
[25] M. C. Clark, L. O. Hall, D. B. Goldgof, L. P. Clarke, R. P. Velthuizen, and M. S. Silbiger, "MRI segmentation using fuzzy clustering techniques," *IEEE Eng. Med., Biol.*, vol. 13, pp. 730–742, 1994.
[26] C. Li, D. Goldgof, and L. Hall, "Knowledge-based classification and tissue labeling of MR images of human brain," *IEEE Trans. Med. Imag.*, vol. 12, pp. 740–750, 1993.
[27] A. Lundervold and G. Storvik, "Segmentation of brain parenchyma and cerebrospinal fluid in multispectral magnetic resonance images," *IEEE Trans. Med. Imag.*, vol. 14, pp. 339–349, 1995.
[28] Z. Liang, J. R. MacFall, and D. P. Harrington, "Parameter estimation and tissue segmentation from multispectral MR images," *IEEE Trans. Med. Imag.*, vol. 13, pp. 441–449, 1994.
[29] W. M. Wells,III, W. E. L. Grimson, R. Kikinis, and F. A. Jolesz, "Adaptive segmentation of MRI data," *IEEE Trans. Med. Imag.*, vol. 15, pp. 429–442, 1996.
[30] M. Ozkan, B. M. Dawant, and R. J. Maciunas, "Neural-network-based segmentation of multi-modal medical images: A comparative and prospective study," *IEEE Trans. Med. Imag.*, vol. 12, pp. 534–544, 1993.
[31] S. C. Amartur, D. Piraino, and Y. Takefuji, "Optimization neural networks for the segmentation of magnetic resonance images," *IEEE Trans. Med. Imag.*, vol. 11, pp. 215–220, 1992.
[32] U. Raff, A. L. Scherzinger, P. F. Vargas, and J. H. Simon, "Quantitation of gray matter, white matter, and cerebrospinal fluid from spin-echo magnetic resonance images using an artificial neural network technique," *Med. Phys.*, vol. 21, pp. 1933–1942, 1994.
[33] N. R. Pal, J. C. Bezdek, and E. C.-K. Tsao, "Generalized clustering networks and Kohonen's self-organizing scheme," *IEEE Trans. Neural Networks*, vol. 4, pp. 549–557, 1993.
[34] K. Cheng, J. Lin, and C. Mao, "The application of competitive Hopfield neural network to medical image segmentation," *IEEE Trans. Med. Imag.*, vol. 15, pp. 560–567, 1996.
[35] T. Kohonen, *Self-Organization and Associative Memory*. New York: Springer-Verlag, 1989.
[36] J. A. Freeman and D. M. Skapura, *Neural Networks: Algorithms, Applications, and Programming Techniques*. Reading, MA: Addison-Wesley, 1991.
[37] S. Haring, M. A. Viergever, and J. N. Kok, "Kohonen networks for multiscale image segmentation," *Image, Vision Comput.*, vol. 12, pp. 339–344, 1994.
[38] E. C. Evans, D. L. Collins, P. Neelin, D. MacDonald, M. Kamber, and T. S. Marrett, "Three-dimensional correlative imaging: Applications in human brain mapping," in *Functional Neuroimaging: Technical Foundations*. Orlando, FL: Academic, 1994, pp. 145–161.
[39] E. F. Jackson, P. A. Narayana, J. S. Wolinsky, and T. J. Doyle, "Accuracy and reproducibility in volumetric analysis of multiple sclerosis lesions," *J. Comput. Assist. Tomogr.*, vol. 17, pp. 200–205, 1993.
[40] G. Gerig, J. Martin, R. Kikinis, O. Kubler, M. Shenton, and F. A. Jolesz, "Unsupervised tissue type segmentation of 3D dual-echo MR head data," *Image, Vision Comput.*, vol. 10, pp. 349–360, 1992.
[41] R. Kikinis, M. E. Shenton, and G. Gerig, J. Martin, M. Anderson, D. Metcalf, C. R. G. Guttman, R. W. McCarley, W. Lorensen, H. Cline, and F. A. Jolez, "Routine quantitative analysis of brain and cerebrospinal fluid spaces with MR imaging," *J. Magn. Reson. Imag.*, vol. 2, pp. 619–629, 1992.
[42] J. P. Guilford, *Fundamental Statistics in Psychology and Education*, 4th ed. New York: McGraw-Hill, 1965.